Radiative exciton recombination and defect luminescence observed in single silicon nanocrystals

Torsten Schmidt,[1,*,†] Alexey I. Chizhik,[2,*,‡] Anna M. Chizhik,[2] Karsten Potrick,[1] Alfred J. Meixner,[2,§] and Friedrich Huisken[1,|]

[1]*Laboratory Astrophysics Group of the Max Planck Institute for Astronomy, Institute of Solid State Physics, Friedrich Schiller University Jena, Helmholtzweg 3, D-07743 Jena, Germany*

[2]*Institute of Physical and Theoretical Chemistry, University of Tübingen, Auf der Morgenstelle 18, D-72076 Tübingen, Germany*

(Received 9 May 2012; published 4 September 2012; publisher error corrected 14 September 2012)

The role of quantum confinement (QC) and surface-related defect centers (DCs) on the photoluminescence (PL) of *individual* silicon nanocrystals (Si NCs) is investigated using confocal microscopy with radially and azimuthally polarized laser beams. It is shown that the multiple-peak PL spectra of single Si NCs revealing SiO_2 phonon side bands are associated with a linear transition dipole moment (TDM) and a short lifetime of 4 ns, indicating that the PL originates from defect centers. In a new study applied to free-standing single Si NCs obtained by Si cluster beam deposition, we could discriminate between PL centers with one- and more-dimensional TDM. Nanoparticles revealing a three-dimensional TDM are characterized by a significantly weaker and structureless Gaussian PL band at larger wavelengths and by μs lifetimes. These PL features are attributed to the radiative recombination of quantum-confined excitons generated in the Si cores. Within the same sample, we found coexistence of Si NCs exhibiting QC PL and others showing DC PL.

DOI: 10.1103/PhysRevB.86.125302 PACS number(s): 78.67.Bf, 78.47.jd, 78.55.Ap

I. INTRODUCTION

Silicon, the element of today's processor technology, still offers a wide and active field of research despite the amazing progress that has been achieved in recent years. Dominating the microelectronics with its exceptional electronic properties, silicon is known to be a poor light emitter because of its indirect band gap structure. Nowadays, due to the dramatically growing information volume, an efficient optoelectronic communication just based on silicon is highly desirable. Therefore, an adequate understanding of the optical properties of nanostructured silicon is essential for designing new devices in photonics and optoelectronics.

Intense visible photoluminescence (PL) from nanostructured porous silicon was observed for the first time in 1990.[1,2] Since that time, research focusing on the optical properties of nanostructured silicon increased dramatically. In particular, silicon nanocrystals (Si NCs), as possible light-emitting sources, gave rise to a still ongoing debate about the origin of their PL. However, reviewing the extensive literature of the past two decades,[3–7] general agreement on the PL processes involved seems to develop. On the one hand, there is the radiative recombination of excitons driven by quantum confinement (QC) and, on the other hand, the PL can arise from defect centers (DCs) in the oxide shell surrounding the silicon core or at the interface between core and shell. Unfortunately, the emitted light arising from both sources may partly cover the same spectral range,[8] making a definitive assignment of the PL very difficult. A recent study by Godefroo *et al.*[9,10] on Si NCs demonstrated that it is possible to control the PL originating from quantum-confined charge carriers and from defect states by hydrogen passivation and UV irradiation, respectively.

Because of their unique optical and chemical properties, Si NCs have been exploited for applications in such diverse fields ranging from optoelectronics[11] and laser physics[12,13] over renewable energies (solar cells[14] and hydrogen production[15]) to biology and medicine, where they are used as nontoxic luminescent labels for DNA molecules,[16] cancer cells,[17] and drugs.[18] Finally, Si NCs are even discussed as carriers for different astrophysical phenomena observed in the Red Rectangle nebula.[19,20] For a recent review about these and other attractive applications of Si NCs, see the book edited by Pavesi and Turan.[21]

The number of publications dealing with single silicon quantum dots is still quite small, but for the past few years, the technique and equipment for high-quality analysis of single quantum dots have made a major step forward. Confocal microscopy especially has become a powerful tool, giving insight into fundamental optical properties. Recently published results on single SiO_2 nanoparticles (NPs)[22] visualized the orientation of the excitation transition dipole moment (TDM) by applying scanning confocal fluorescence microscopy in combination with higher-order laser modes.[23,24] Confocal PL spectroscopy of single Si NCs[7] and SiO_2 NPs[22] revealed surprising similarities in the emission characteristics of both kinds of nanoparticles. When probing single Si NCs, the studies[7] suggested a transition of the PL originating from radiative recombination of charge carriers in a quantum-confined system for larger Si NCs to radiative mechanisms related to various defects at the interface or in the shell of small Si NCs. This transition was interpreted as the so-called "breakdown of QC" caused by surface-related defect centers appearing as inner-band-gap states for Si NCs with diameters smaller than $\sim$2.7 nm.[4,7]

The present study is focused on the PL characteristics of individual Si NCs with lateral dimensions between 2 and 8 nm, synthesized by laser-induced pyrolysis of SiH_4.[25–28] It is a new application of the previous work that was devoted to single SiO_2 NPs,[22,29] employing the same methods. Moreover, it can be considered as an extension of the earlier work of Martin *et al.*[7] on Si NCs, yielding additional and new information on the transition dipole moment for excitation and on the fluorescence lifetime of single NPs. As the Si NCs and SiO_2 NPs were investigated with the same equipment and under the same conditions, it is now possible to compare the optical properties of both systems on the single-particle level.

Comparing Si NCs with SiO_2 NPs, one should always be aware of the fundamental difference between these two

nanomaterials. Whereas the Si NCs we are dealing with contain a crystalline Si core that is surrounded by an amorphous layer of SiO_2, the SiO_2 NPs are completely oxidized and amorphous. Therefore, we distinguish semantically between nanocrystals (i.e., Si NCs) and nanoparticles (i.e., SiO_2 NPs). While the PL of SiO_2 NPs definitely results from defects, the PL of Si NCs can have the two different origins discussed (QC and DCs). Note that the smaller the Si NCs are, the more important the SiO_2 shell is. As a result, one can expect that the contribution of defect PL becomes increasingly more important with decreasing size of the Si NCs. In this sense, the SiO_2 NPs can be considered as Si NCs with vanishing core.

After having characterized the rather strong defect-based photoluminescence (DC PL) of polymer-embedded Si NCs described only briefly here, we focused on the observation of PL arising from exciton recombination in single Si NCs, which is expected to be much weaker due to the long radiative lifetime. Employing longer integration times and significantly lower laser power to reduce bleaching and interference with background fluorescence, we were indeed able to observe red PL from individual Si NCs.

II. EXPERIMENTAL METHODS

A. Synthesis of Si NCs

High-quality silicon nanocrystals (Si NCs) were synthesized by laser-induced pyrolysis using silane (SiH_4) as gaseous precursor.[25–28] The dissociation of SiH_4 takes place in a gas flow reactor and is accomplished by the infrared radiation of a line-tunable CO_2 laser (Urenco, model ML 104; repetition rate, 20 Hz; pulse width, 150 ns; emission wavelength, 10.6 μm), which provides a very steep temperature gradient ensuring that the reactions take place in a wall-less environment. The molecular flow emanating from the inner gas inlet is crossed perpendicularly by the focused laser radiation inducing the decomposition of SiH_4 followed by gas-phase condensation and subsequent formation of crystalline silicon quantum dots. The Si NCs are collected as nanopowder in a filter assembly at the exit of the gas flow reactor. The following process parameters were used for the present study: total (constant) pressure inside the flow reactor: 330 mbar; SiH_4 flow rate: 30 sccm; He flow rate: 1100 sccm; pulse energy of the CO_2 laser: 45 mJ (sccm denotes standard cubic centimeter per minute).

B. Sample preparation from Si nanopowder

For the investigation of single Si NCs from powder samples collected in the filter, the nanoparticles were embedded at very low concentration into a polymer matrix. Dispersing a small amount of the nanopowder in toluene and mixing the dispersion with either poly(methyl methacrylate) (PMMA, $[C_5O_2H_8]_n$) or polystyrene (PS, $[C_8H_8]_n$), a droplet (10 μl) of the resulting mixture was spin coated onto a clean quartz cover slide (thickness 170 μm). The thickness of the polymer film was determined by atomic force microscopy to be 50–60 nm. As confocal microscopy is used as standard tool for the investigation of fluorescent dye molecules, contamination of the polymer by impurities (e.g., fluorescent dye molecules) was excluded by spectroscopic verification of a spin-coated droplet of the polymer without Si NCs.

C. Sample preparation by cluster beam deposition

The flow reactor for gas-phase condensation is mounted into the source chamber of a cluster beam apparatus.[26,27,30] A conical nozzle with an aperture of 200 μm extracts the as-synthesized Si NCs from the reaction zone and expands them with helium as carrier gas into the evacuated source chamber. Employing a skimmer and differential pumping, a molecular beam of freely propagating Si NCs is formed. The size of the NCs is determined *in situ* by time-of-flight mass spectrometry. Very low-coverage deposition in single-particle concentration is achieved by using a fast-switching shutter, which opens the cluster beam such that only one or another given number of Si NC pulses are transmitted and deposited onto the substrate.

D. Confocal microscopy

The basic optical setup for fluorescence spectroscopy has already been described in the main article and in the Supplemental Material[31] to the paper on single SiO_2 NPs.[22] A schematic diagram of the setup is shown in Fig. 1. Photoluminescence decay measurements of single nanoparticles (Si NCs and SiO_2 NPs) have been carried out with a home-built confocal laser scanning microscope[22,29] based on a Zeiss Axiovert 135 TV equipped with a fluorescence lifetime imaging module (FLIM) (Picoharp 300, Picoquant). The focusing of the excitation light and the collection of the fluorescence were accomplished with a microscope objective (Plan-Neofluar, $100\times/\mathrm{NA} = 1.25$ oil immersion, Zeiss). The excitation and fluorescence light were separated by a dichroic beam splitter (FT500). For sample scanning, a feedback-controlled sample stage (E-710.3CD, PI) with nanometer precision was utilized. A pulsed diode laser (LDH-P-C-470, Picoquant) operated at 473 nm was used as an excitation source. Backscattered excitation light was blocked by a steep-edge filter (LP02-473RU-25, Semrock). The fluorescence light was focused onto the active area of a spectrally integrating avalanche photodiode (SPCM 200, Perkin Elmer). Data acquisition was accomplished with a commercially available software package (SymPhoTime, Picoquant).

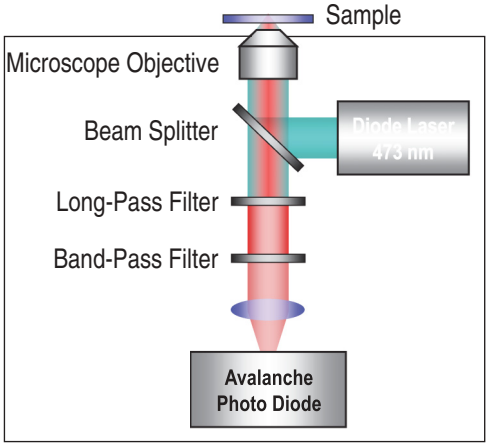

FIG. 1. (Color online) Schematic view of the confocal microscopy setup used for fluorescence decay measurements.

III. RESULTS AND DISCUSSION

A. Fluorescence studies on single Si NCs embedded in a polymer

To clarify the origin of the PL of single Si NCs (QC vs. DCs) and to reveal possible similarities with results recently published on single SiO_2 NPs,[22] confocal microscopy was carried out under the same experimental conditions as used for the investigation of single SiO_2 NPs.[22,29] Starting with confocal fluorescence imaging, the characteristics of the transition dipole moment (TDM) for the excitation of single Si NCs were recorded to yield information on the excitation process being involved.

The TDM differs in its dimensionality for the excitation of strongly localized defect states (DC PL) and excitonic excitation (QC PL). While defect centers reveal a linear one-dimensional TDM,[22] the latter one is associated with a degenerate, three-dimensional TDM isotropically distributed in space,[32–34] resulting from the spherical structure of our Si nanocrystals.[35] Using higher-order laser modes, i.e., an azimuthally (APLB) or radially polarized laser beam (RPLB),[23,24] the appearance of specific fluorescence patterns visualize the dimensionality and the spatial orientation of the excitation TDM. For instance, in the case of APLB excitation, a horizontally oriented one-dimensional TDM gives rise to a pattern consisting of two nearby bright spots of elliptical shape resembling a coffee bean, while a three-dimensional TDM causes a fluorescence pattern of ringlike shape.[34] When RPLB is employed, the out-of-plane component of the TDM, and, therefore, its three-dimensional orientation, can be determined in addition. Details of this technique and its application to the visualization of NPs are reported in Refs. 22,29, and 34.

The Si NCs were embedded in a polymer layer, either PMMA or PS, and excited with the mode-converted beam of an Ar ion laser ($\lambda_{exc} = 488$ nm).[22] Fluorescence images were obtained from more than 300 single Si NCs. All of them exhibited coffee bean patterns. The images recorded from Si NCs were identical with those observed for SiO_2 NPs.[22] Moreover, they showed the same dynamical behavior as far as fluorescence intermittency and transition dipole moment flipping are concerned.[22] An example for a continuous series of fluorescence excitation images obtained from an individual Si NC embedded in PMMA is given in the Supplemental Material.[36]

The observed sharp patterns clearly show that single nanocrystals were detected and that the PL signal originated from only one luminescence center. In order to demonstrate the single-particle character by other means, time traces of the PL signal were recorded using a linearly polarized Gaussian laser beam for excitation. These time traces showed the typical two-level blinking behavior (fluorescence intermittency) on a time scale of seconds. Again, an example can be found in the Supplemental Material.[36]

Since the present study was carried out with the same confocal microscopy setup as was used for the investigation of single SiO_2 NPs[22] a comparison with the recently published PL spectra of SiO_2 NPs will be most meaningful. Furthermore, employing a similar preparation technique, the observed charge carrier localization (electron-phonon coupling to Si-O-Si phonons) accompanied by the "breakdown of the quantum confinement" in small single Si NCs reported in the work of Martin *et al.*[7] should be verified.

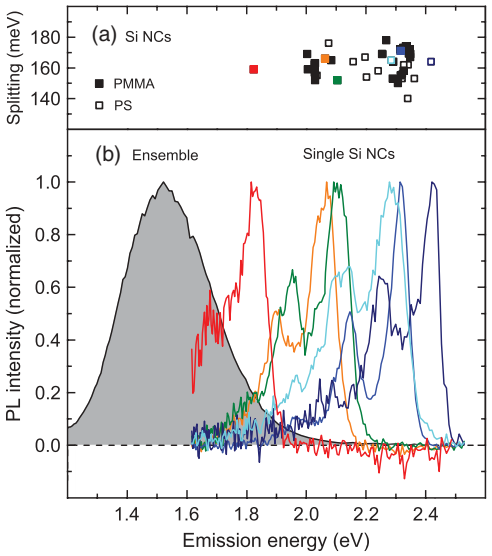

FIG. 2. (Color online) PL spectra of individual Si NCs. (a) Splitting between zero-phonon line and first phonon band as a function of zero-phonon line energy for *all* Si NCs investigated. Truncated spectra with zero-phonon lines above 2.5 eV were not considered (see text). Solid and open symbols refer to Si NCs embedded in a PMMA or PS matrix, respectively. (b) Set of selected single Si NC spectra including those with the lowest and highest zero-phonon line energy observed below 2.5 eV. The single-particle spectra are compared with the ensemble spectrum of the Si nanopowder from which the microscopy samples were prepared. Splittings shown in color in panel (a) refer to the individual spectra displayed in the same color in panel (b).

Figure 2(b) shows a selection of six full spectra taken from individual Si NCs embedded in PMMA or PS as polymer matrix. All spectra are characterized by a zero-phonon line featuring the highest intensity and one or two phonon bands at lower energy. Originally, the spectra were measured as a function of wavelength. To transform them from wavelength scale to energy scale, the intensities were multiplied by the proper Jacobian. Prior to this transformation, the PL curves were corrected for the wavelength-dependent detection sensitivity of the CCD chip and the transmission of the optical components, including the beam splitter and the long-pass filter used to suppress the light from the excitation laser. For details, e.g., on the window for observation defined by the latter two components, see the Supplemental Material.[36]

As can be seen in Fig. 2(b), all spectra (except of one) display their maxima (zero-phonon lines) in the narrow range between 2.0 and 2.5 eV. It should be noted that we observed also a few Si NCs emitting at higher energy; but since the positions of their zero-phonon lines could not be determined because they fell outside the observation window, they were not considered in Fig. 2(b). On the lower-energy side, we found only one Si NC with PL maximum below 2 eV [red spectrum in Fig. 2(b)].

The PL ensemble spectrum (integrated over several thousand Si NCs) of the Si nanopowder, from which the samples for confocal microscopy were prepared, is also shown in Fig. 2(b) (black curve with gray area). It was measured with the same high-repetition diode laser used for recording the

single-particle PL spectra. As expected, the ensemble spectrum is much broader and does not reflect the phonon bands. However, it is striking that the maximum of the ensemble spectrum is at much lower energy than the majority of single-particle spectra.

The separations between the zero-phonon line and the first phonon band are plotted as a function of the zero-phonon line position in Fig. 2(a). The colored data points refer to the spectra displayed in the panel below. Solid squares are obtained from Si NCs embedded in PMMA while open squares refer to NCs in PS. It is seen that the splitting between zero-phonon line and first phonon band varies between 140 and 180 meV for all investigated Si NCs. If we compare the present results with those obtained for completely oxidized SiO_2 NPs (see Fig. 5 of Ref. 22) the similarity between both sets of data is striking, even if the details of the spectral features (splitting, amplitude ratio, and spectral range) are considered. Finally, it is noted that the present Si NC spectra are also almost identical to those of Martin *et al.*,[7] proving that consistent results are obtained with different setups. Only the increase of the splitting between the zero-phonon line and the first phonon band with increasing energy is somewhat less pronounced in our study. In all three studies just discussed, the distribution of phonon energies is located around 160 meV, allowing us to attribute the observed phonons to the longitudinal optical mode (LO_3 transition) in SiO_2.[37] Thus, the low-energy satellite peaks observed in Si NCs and SiO_2 NPs manifest that the photoemission is often accompanied by the simultaneous excitation of one or two LO_3 phonon quanta. Regarding the abundance of single Si NCs observed within a small energy interval, as discussed by Martin *et al.*[7] in their Fig. 3, our study reveals similar characteristics. As can be seen in Fig. 2(a), where we have plotted the phonon splitting for all Si NCs investigated, we observe two accumulation points, one between 2.0 and 2.1 eV and the other at 2.3 eV.

Important information on the nature of the PL center is also expected from decay lifetime measurements, which, however, are difficult to perform for single particles. The main interest of this experiment was to find out whether phonon-coupled transitions are associated with different (perhaps shorter) lifetimes compared to zero-phonon transitions. Due to the low signal level, it was not possible to measure the PL decay for every wavelength emitted by the individual Si NC. Instead, we used a set of optical band-pass filters (transmission: ~98%), covering the entire spectral range of interest (500–650 nm). As an example, Fig. 3(a) shows the PL spectrum of a Si NC, which we have analyzed in this way. The ranges of transmission with $T > 50\%$ are given by the colored areas denoted F_1–F_6. If, in the example of Fig. 3(a), filter F_2 is used, only photons belonging to the zero-phonon line can reach the detector. On the other hand, with filter F_4, only photons which were involved in the excitation of a phonon will be analyzed.

Figure 3(b) presents the decay curves actually measured with the different filters. The main frame displays the curves with linear y axis, while the inset shows the same curves in a semilogarithmic representation. The black curve has been measured without any filter in the optical path (referred to as F_0), and the colored decay curves were obtained with the filters F_1–F_6, whose transmission ranges are given in Fig. 3(a) in the same color. As can be seen from the inset

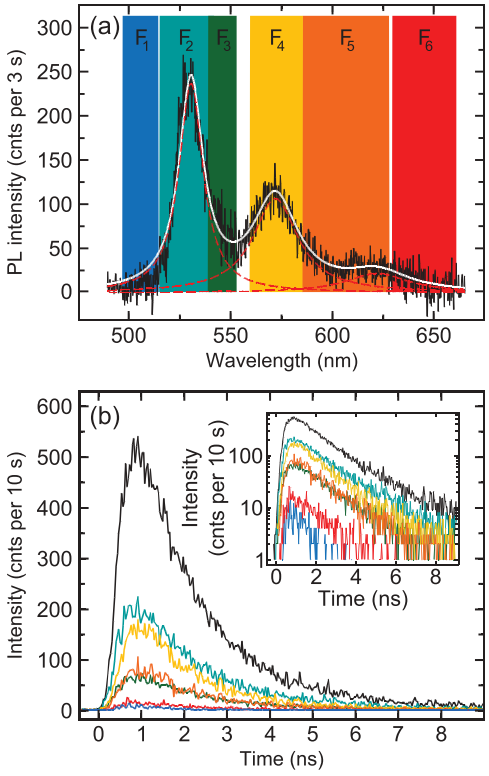

FIG. 3. (Color online) PL spectrum of a single Si NC in PMMA and PL decay curves measured in various spectral ranges. (a) The black curve shows the PL spectrum of a single Si NC embedded in a PMMA matrix. To unravel the different contributions, the spectrum was fitted by a set of three Gaussians (red dashed lines), which add up to yield the white solid curve. The colored areas represent the transmission ($T > 50\%$) regimes of various optical band-pass filters (F_1–F_6) used to carry out lifetime measurements for a particular narrow range of emission wavelengths. (b) Six single Si NC PL decay curves measured with the filters F_1–F_6. The various colors of the curves correspond to the colors used to characterize the transmission of the respective filters in panel (a). The black decay curve was measured without filter. The inset shows the same data but with the intensity plotted in logarithmic scale.

in Fig. 3(b) (semilogarithmic representation), all decay curves reflect a monoexponential decay, suggesting that the signal was emitted by a single NP. Fitting the decay curves with exponentials $A_i \exp(-t/\tau_i)$, we obtained the following seven lifetime values: $\tau_0 = 1.59$ ns, $\tau_1 = 1.33$ ns, $\tau_2 = 1.70$ ns, $\tau_3 = 1.68$ ns, $\tau_4 = 1.53$ ns, $\tau_5 = 1.55$ ns, and $\tau_6 = 1.59$ ns. Taking into account the signal-to-noise level, the experimental error is estimated to be 0.15 ns. Within this experimental uncertainty, all lifetimes derived for this specific Si NC in different spectral ranges can be considered to be equal. Averaging over all values, we obtain as average lifetime for this specific Si NC $\tau_{av} = (1.55 \pm 0.15)$ ns. The fact that τ_1 falls outside the experimental error can be explained by the very low signal which makes a precise determination of the PL lifetime impossible. The consistency between the PL spectrum and the decay curves has been verified by determining the integrated intensities of the different contributions in the PL spectrum and the decay data.

As the phonon coupling was found to have no effect on the lifetime, further decay measurements for 156 individual

Si NCs and 43 SiO_2 NPs were carried out without filters. In all cases, we observed single exponential decays with lifetimes between 1 and 13 ns. The lifetime distributions derived from this extensive data set yield an average lifetime of 4 ns for both kinds of nanoparticles. The full data can be accessed in the Supplemental Material.[36]

Summarizing the most important results presented up to now, we state that we were able to visualize the TDM for the excitation of single Si NCs, that the TDM is linear (and not two- or three-dimensional) and isotropically distributed, and that dynamical effects typical for single particles like TDM flipping, fluorescence intermittency, and photobleaching are observed. The spectroscopic characterization of individual Si NCs reveals PL spectra with narrow zero-phonon line and phonon bands, which can be associated with the excitation of longitudinal optical phonons in the SiO_2 shell. The spectra are essentially identical to the PL spectra of an earlier study on single Si NCs by Martin *et al.*[7] and those of a very recent study of El-Kork *et al.*[38] carried out in the same laboratory. Moreover, they are also identical to the PL spectra of single SiO_2 NPs published by Chizhik *et al.*[22] The maxima of almost all PL spectra observed from single Si NCs fall into an energy range between 2.0 and 2.5 eV. This range does not match the range covered by the ensemble of Si NCs (1.2–2.0 eV), from which the microscopy samples were made, nor does it match the fluorescence range observed in experiments with size-dispersed samples of Si NCs.[39] Fluorescence decay measurements carried out for both single Si NCs and single SiO_2 NPs reveal equal decay characteristics and yield lifetimes of the order of 4 ns. Particularly important may be the result that phonon coupling does not result in a shorter lifetime. Finally, it is emphasized that the short fluorescence lifetime is not compatible with exciton recombination in Si quantum dots, which is characterized by lifetimes on the order of microseconds.[28,40] Considering all results just discussed, we come to the conclusion that the PL observed in the present study from single Si NCs cannot be associated with radiative recombination of quantum-confined excitons (QC PL); instead, it must be attributed to fluorescence arising from local defect centers in the interface between the Si core and the SiO_2 shell, in the SiO_2 shell, or in the interface between the SiO_2 shell and the polymer host matrix.

B. Fluorescence studies on single Si NCs prepared by cluster beam deposition

The results presented until now clearly demonstrate identical optical properties for single SiO_2 NPs and Si NCs when they are embedded in a polymer (PMMA or PS) matrix. This finding suggests that the emission process in both kinds of nanosystems is governed by the same mechanism, namely defect luminescence. Imaging the transition dipole moment characteristics of individual Si NCs, the expected ringlike pattern indicating exciton creation in spherical semiconductor quantum dots was not observed at all.[32–34] Furthermore, PL spectra peaking in the red to near infrared spectral range, typical for QC PL, could not be detected. Nevertheless, this cannot be taken as a serious proof that defect-based PL is the only emission mechanism and that excitonic PL can be excluded.

Regarding the standard method of sample preparation for confocal microscopy, which consists of dispersing the species to be examined in toluene and embedding them at very low concentration into a thin polymer film, we cannot exclude that the as-prepared crystalline Si NCs have experienced further oxidation to become SiO_2-like NPs. In any case, it should be emphasized that the distinction between Si NCs with a native oxide shell and pure SiO_2 NPs is questionable if the volume of the crystalline core becomes comparable or even smaller than the volume of the oxide shell. In that case, it is very likely that the PL dynamics are mainly governed by the shell.

To overcome the obstacle of this standard method of sample preparation, an alternative approach was conceived to avoid any unintentional chemical surface modification of our Si NCs. Apparently, confocal microscopy of single Si NCs requires low particle density in conjunction with relatively large spacings between the individual particles. For the purpose of preparing an adequate sample, the facilities of a cluster beam apparatus equipped with time-of-flight mass spectrometer (TOF-MS) were used to enable a matrix-free deposition of the as-synthesized Si NCs in single-particle concentration. A description of the experimental details on the synthesis of Si NCs by laser pyrolysis in conjunction with cluster beam extraction can be found elsewhere.[26,27,30] Due to the fact that, for small Si NCs with a diameter <2.7 nm, the PL process is governed by surface states,[4] the synthesis conditions were chosen such that the final size of the as-prepared Si NCs did not match the critical size regime below 3 nm. According to the TOF-MS spectra measured *in situ*, the calculated size distribution[25] is characterized by an average particle diameter of 4.0 nm and a full width at half maximum (FWHM) of 1.1 nm. However, due to the reduced sensitivity of the channel plates, which is more pronounced for the larger Si NCs, the quoted average size should rather be considered as a lower limit.

To verify the required low coverage and to determine the average number density of the deposited nanocrystals, AFM measurements were carried out. Typically, the topographic image of Si NCs deposited on a mica substrate reveals an average particle concentration of 0.44 particles per μm^2, with a separation of several hundred nanometers (see the Supplemental Material).[36] Such a coverage is perfectly suited for single-particle spectroscopy.

In addition to providing sufficiently low coverage, the recording conditions were adapted to search for single Si NCs revealing QC PL. Photoluminescence arising from exciton recombination in Si NCs is characterized by a rather long radiative lifetime (>1 μs),[28] and, therefore, the signal is expected to be much weaker than that we have encountered before. The signal-to-noise level was improved by employing longer integration times per pixel (fourfold increase) and lower laser power (decrease by a factor of 3 to 4). During the first recording, a major drawback emerged, namely extensive bleaching, due to the missing polymer matrix previously acting as protective layer. The strong bleaching was reduced by recording the fluorescence images under a continuous flow of nitrogen.

With respect to the points discussed above, we were eventually able to observe QC PL from individual Si NCs, as illustrated in Fig. 4. The fluorescence images in Figs. 4(a)

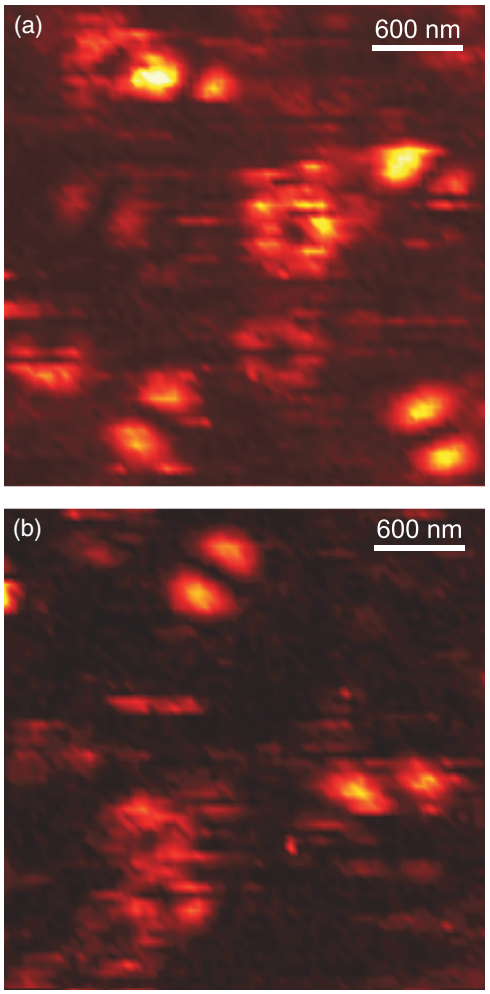

FIG. 4. (Color online) Fluorescence microscopy images of free-standing Si nanocrystals. The fluorescence images (a) and (b) depict different sample areas, each probing $3.2 \times 3.2\ \mu m^2$. The images were obtained by scanning through the focal region of an azimuthally polarized laser beam (APLB). They reveal the excitation patterns of several individual, free-standing Si NCs (deposited on a quartz cover slide by the cluster beam technique). Two kinds of excitation patterns (coffee beans and ringlike structures) can be distinguished.

and 4(b), obtained under excitation with azimuthally polarized laser beam (APLB), each show a different sample area of $3.2 \times 3.2\ \mu m^2$. Several excitation patterns clearly resembling a coffee bean or a ring structure can be observed. Besides the two prominent ring patterns in the center of Fig. 4(a), three closely spaced Si NCs are found in the lower left of Fig. 4(b), which clearly exhibit a more-dimensional TDM. As already mentioned, the visualization of the TDM using higher-order laser modes for excitation allows us to identify the origin of the observed PL in one single Si nanocrystal. For APLB excitation, defect-related PL is associated with a coffee bean pattern (pointing to a 1d TDM)[22] while quantum-confined PL gives rise to a ringlike structure (indicating a 3d TDM).[32–34]

For the following discussion, it should be kept in mind that the present free-standing Si NCs consist of a crystalline Si core surrounded by a native layer of SiO_2. All nanocrystals experienced the same history, i.e., after synthesis, they were all subjected to the same gentle oxidation in ambient air. Furthermore, the information given by each fluorescence image was obtained within one single scan. Thus, we can clearly state a coexistence between individual Si NCs exhibiting QC PL and others showing defect luminescence within the same sample. Regarding the abundance of coffee beans and rings, defect-based PL is observed 1.5 times more frequently (despite the careful preparation and a rather large mean particle size of 4.0 nm). It is interesting to note that, in the present study, a switching from a ringlike structure to a coffee bean pattern could be observed only once during the course of two consecutive scans. This shows that both DC PL and QC PL may occur in one and the same particle and that both mechanisms could be indeed competing processes.

Comparing the stability of the fluorescence patterns of both recombination processes, it is clearly observed that, in the case of quantum confinement, fluorescence intermittency (blinking) occurs more frequently. The interruption by many dark periods results in a poor depiction of the ringlike structure. In order to visualize the frequent blinking with higher resolution, the number of pixels per fluorescence image was increased by a factor of 4. An image series recorded at high resolution employing both polarization modes (APLB and RPLB) can be viewed in the Supplemental Material.[36]

As can be seen in Fig. 4, the intensity of the coffee bean- and ringlike fluorescence patterns is more or less equal even though the defect-based PL is characterized by a short lifetime so we would expect stronger fluorescence intensity than for QC PL. This can be explained as follows. First, in contrast to polymer-embedded nanocrystals, a preferred orientation of the TDM pointing towards the substrate can be assumed due to the breaking of symmetry. The free-standing NCs are attached directly to the substrate surface (SiO_2) and out-of-plane (almost vertical) orientations of the TDM may prevail, resulting in weaker coffee bean images under APLB excitation. An example for this observation is shown in the Supplemental Material[36] (Fig. S5). Second, due to the reduced laser power, the excitation rate is lower and, thus, the effect of enhanced intensity for fast recombination processes is diminished. As a result, comparable photon emission (equal intensity) can be rationalized for both processes.

In order to meet the rather long lifetime of quantum-confined PL, the acquisition time for recording PL spectra was set to 10 min. The series of PL spectra shown in Fig. 5(a) was acquired from the same sample just discussed. The PL spectra were corrected for the wavelength-dependent detection sensitivity of the setup and transformed to energy scale using the proper Jacobian. Compared to the spectra shown in Fig. 2, the present PL curves are characterized by significantly weaker intensity and a structureless Gaussian PL band shifted to the red. The emission range covered by the measured spectra is typical for QC PL of oxygen-passivated Si NCs.[39] Fitting the PL curves with single Gaussians [blue curves in Fig. 5(a)] and using the formula of Delerue *et al.*,[41] the size of the crystalline Si cores can be determined. With $E_{PL} = 1.11 + 3.73\, d^{-1.39}$ in which E_{PL} are the maximum position of the PL curve in eV, 1.11 [eV] the bandgap of bulk Si at 300 K, and d the core diameter in nm, we calculated particle sizes varying from 3.4 to 4.1 nm. The specific Si NC size is indicated in Fig. 5(a) for each PL curve.

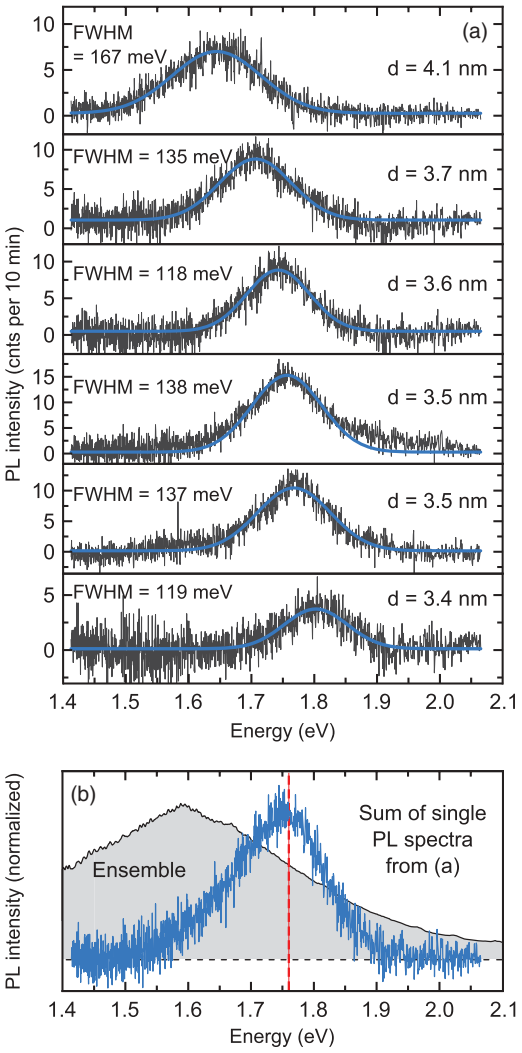

FIG. 5. (Color online) Series of PL spectra of free-standing Si NCs. (a) The single-particle PL spectra are characterized by a structureless single Gaussian-type PL band in the red spectral range. The PL curves were fitted with single Gaussians (blue curves). For each PL measurement, the specific particle size as derived from the peak position is given. (b) Comparison between the PL spectrum observed for an ensemble of Si NCs (black curve with gray shaded area) and the sum of all measured single-particle spectra (blue curve). The ensemble spectrum is much broader and peaks at lower energy. The dashed red line marks the position of emission energy (1.76 eV), for which the Si NCs were found to have their highest PL yield.[39]

In Fig. 5(b), a PL spectrum of the corresponding Si NC ensemble (black curve with gray-shaded area) and the sum of all measured single-particle spectra of Fig. 5(a) (blue curve peaking around 1.75 eV) are plotted for comparison. The ensemble, a thicker layer of Si NCs deposited on a fused silica window, was prepared during the same experimental run as the sample for single-particle spectroscopy and under identical synthesis conditions. Moreover, for recording the ensemble spectrum, we used the same experimental setup as for single-particle spectroscopy. As can be seen in Fig. 5(b), the ensemble PL is much broader and peaks at longer wavelengths. The slight mismatch between the ensemble PL and the sum of single-particle spectra cannot be explained by a resonant energy transfer mechanism[42,43] as we found no evidence of such effect when we compared the PL of samples with very low and very high Si NC coverage.[44] In contrast, we are led to explain the mismatch of the PL curves in Fig. 5(b) by the fact that the brightness of a NC depends on the emission wavelength. The highest PL quantum efficiency was found for Si NCs with a diameter of 3.5 ± 0.5 nm.[39] The corresponding emission energy (1.76 eV) is marked in Fig. 5(b) by the dashed red line. Considering the fact that single-particle detection relies on strong light emitters, only the most efficient light emitters will be detected, and it is therefore conceivable that particles with less efficient light emission have escaped detection. As a result, it can be understood that the measured single-particle PL spectra show up in a narrow emission range around 1.76 eV.

The widths (FWHMs) of the single-particle PL bands are also given in Fig. 5(a). Varying from 118 to 167 meV, they are somewhat broader compared to an earlier study by Valenta *et al.*,[45] who used a top-down method to produce an array of single Si quantum dots. In this context, it should be noted that newer low-temperature studies of the Linnros group revealed linewidths as small as 2 meV at 35 K.[46] An even newer publication by Sychugov *et al.*[47] demonstrated the coexistence of 10 K single-particle spectra consisting of sharp zero-phonon lines and spectra exhibiting an additional TO phonon replica 60 meV below the zero-phonon transition. The room temperature conditions in our study do not allow to resolve this TO phonon band, but it could be hidden in the low-energy tail of the spectra shown in Fig. 5(a). Another recent study on single Si NCs by El-Kork *et al.*[38] reports spectral diffusion of approximately 20 meV within an acquisition time of several seconds. Their data are also consistent with the occurrence of a Si phonon replica around 56 meV. Phonon coupling is discussed in greater detail in Refs. 48 and 49.

A second sample, prepared under slightly different synthesis conditions, confirmed the results shown in Fig. 5. Here, the average particle diameter calculated from the measured single PL spectra varied between 3.6 and 4.2 nm while the FWHMs covered a range from 121 to 154 meV.

Different PL mechanisms are observed to coexist within the same sample but pertain to different Si nanocrystals. Therefore, it is desirable to perform combined spectrally resolved and time-resolved PL measurements on the same free-standing Si NC, in order to prove whether quantum-confined PL and defect luminescence can be distinguished in both frequency and time domain. The results of such study are summarized in Fig. 6. Figure 6(b) shows a typical fluorescence image obtained by scanning the sample with the Gaussian beam of a pulsed diode laser. It reveals in grayscale the intensity patterns of different Si NCs located within the scanned sample area. The single-particle character of these luminescence centers was verified by recording time traces which clearly exhibited a two-level blinking behavior. As mentioned before, fluorescence processes associated with short lifetimes (DC PL) give rise to more efficient light emitters than those with long lifetimes (QC PL). Thus, considerable differences in intensity indicate (in the case of high excitation laser power) recombination processes running on different time scales. To verify this assumption, PL spectra and decay curves were recorded from two luminescent nanoparticles, one with high intensity and

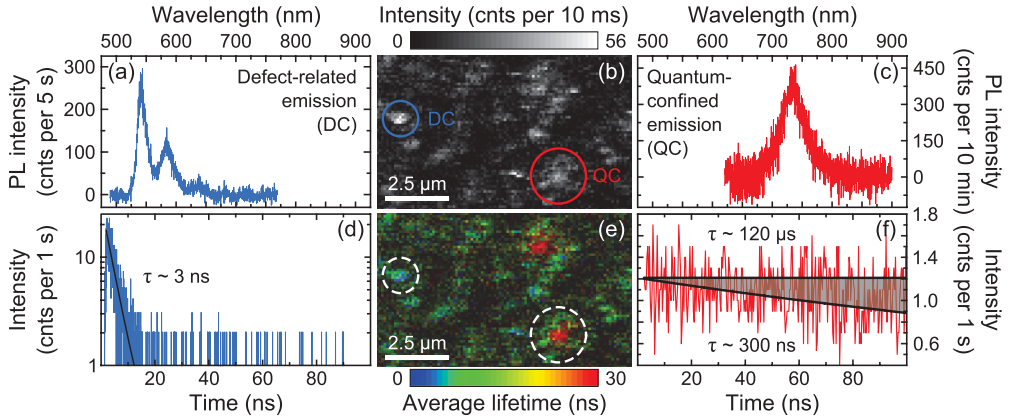

FIG. 6. (Color online) Spectrally and time-resolved PL measurements on free-standing Si NCs. (b) The fluorescence image obtained by excitation with a Gaussian laser beam reveals the intensity patterns of different individual Si nanoparticles. The PL spectra of the particles marked by the blue (particle with high intensity) and red circles (particle with lower intensity) are given in panels (a) and (c), respectively. It is evident, that two different PL mechanisms are operative. Frame (e) displays a lifetime image (in false colors) of the same area given by the intensity image in panel (b). The corresponding decay curves for the encircled blue and red particles are shown in (d) and (f), respectively. The black curves in frame (f) indicate a lower (300 ns) and an upper limit (120 μs) of the lifetime compatible with the measured decay curve.

one with considerably lower intensity, each highlighted in the fluorescence image [Fig. 6(b)] by a blue (DC) and red (QC) circle, respectively. The corresponding PL spectra are plotted on either side of the fluorescence image. On the left-hand side [Fig. 6(a)], the PL spectrum acquired from the particle featuring high PL intensity is plotted in blue while, on the right-hand side [Fig. 6(c)], the red PL spectrum recorded from the low-intensity spot is shown. It is evident, that both luminescence centers are characterized by significantly different PL spectra. Whereas the left spectrum is practically identical to those presented in Fig. 2, the right spectrum falls into the red-to-infrared spectral range typical for QC PL and resembles the data shown in Fig. 5(a). Note that the PL intensity scales of both spectra differ by two orders of magnitude.

Since the confocal microscope is equipped with a fluorescence lifetime imaging microscopy (FLIM) modul, the PL decay can be monitored for each pixel. Details on the FLIM modul and the software-based analysis are given in Sec. II. The lifetime image that corresponds to the intensity image (b) is shown in the middle of the lower panels. As can be seen from the false color scale, the two luminescence centers discussed before are related to significantly different fluorescence lifetimes. The bright spot in the upper image has turned into a blue-colored spot, indicating fast decay, while the weakly luminescing spot became red as it is associated with a much longer lifetime. Note that the real lifetime of the red nanoparticle is actually much longer than the 30 ns indicated by the color scale.

This statement can be corroborated by analyzing the PL decay curves belonging to each single particle marked by the dashed white circles. The fluorescence decay curves for the blue and red spots are plotted on either side of the lifetime image, in Fig. 6(d) for the blue and in Fig. 6(f) for the red nanoparticle. The decay curve in Fig. 6(d) exhibits the same temporal behavior as observed for Si NCs and SiO_2 NPs embedded in a polymer matrix (see Fig. 3). The monoexponential decay confirms that a single nanocrystal was detected, and its fit yields a fluorescence lifetime of 3.2 ns. In contrast, the decay associated with QC PL shows no clear signal decrease. Since we used for these spectroscopic measurements a diode laser with a repetition rate of 10 MHz, the separation between two consecutive laser shots was 100 ns. It is obvious that radiative recombination processes slower than 100 ns cannot be properly measured as they fall outside the time gate of the instrument. From lifetime studies on Si NC ensembles, it is known that the average lifetime is a function of the emission energy, which, in turn, depends on the nanocrystal size.[28] Taking the measured single Si NC PL spectrum from Fig. 6(c) as reference, we derive from the peak position at 730 nm a more realistic lifetime of about 120 μs. In order to show that this decay time is not in contradiction of the recorded decay curve, a simple exponential function with a lifetime of 120 μs is drawn into Fig. 6(f) (representing the upper limit of the gray-shaded area). A second decay curve, corresponding to a lifetime of 300 ns, marks the lower limit of the gray-shaded area. Hence, the measured data are compatible with a lifetime between 300 ns and 120 μs.

C. Discussion

Using confocal microscopy, we have investigated the PL properties of single Si NCs both embedded in a polymer matrix and as free-standing species on a fused quartz window. The single-particle character is strongly supported by the following observations: (1) Applying azimuthally and radially polarized laser beams, the orientation and dimensionality of the excitation transition dipole moment of single nanoparticles could be visualized. The sharp images prove that single-particle TDMs are visualized. (2) PL time traces show the switching between ON and OFF states that is characteristic for fluorescence intermittency in single nanoparticles. (3) PL spectra attributed to defect luminescence reveal narrow zero-phonon lines ($<$100 meV) in the green with well-resolved phonon bands. (4) Finally, in a semilogarithmic representation, the measured decay curves can be fitted by straight lines, indicating that the excited state can be associated with a single lifetime.

In the beginning of the experiments, when we were dealing with polymer-embedded Si NCs, we found remarkably close agreement with the results previously obtained from SiO_2 NPs using the same sample preparation technique and the same microscopy setup:[22]

(1) Experiments visualizing the TDM for excitation yield exactly the same results for both nanosystems. Most noteworthy is the fact that the TDM is one-dimensional. In addition, as reported for SiO_2 NPs,[22] the transition dipole moment for emission is found to have the same orientation as the TDM for excitation. Finally, no difference is found as far as dynamical processes like TDM flipping, fluorescence intermittency, and bleaching are concerned. These findings suggest that the PL results from defect centers (DC PL) rather than from the radiative recombination of charge carriers in a quantum-confined system (QC PL). For instance, we sometimes observed a sudden flipping of the TDM, which is not compatible with the quantum confinement picture. However, TDM flipping can be understood when defect centers (DC) are responsible for the PL. In that case, two or even more DCs existing in the shell or at the interface of the same particle could be operative one at a time. TDM flipping can then be explained by charge fluctuations in the matrix environment of the NP affecting the energy levels of the DCs and, thus, favoring the activation of different DCs, depending on the situation. It should, however, be emphasized that the nanoparticles usually have only *one* active defect; otherwise they could not feature molecule characteristics.

(2) Spectrally and time-resolved PL measurements reveal the same optical behavior. The shapes of the spectra are identical; they are both composed of a zero-phonon line and two phonon bands at lower energy associated with the excitation of longitudinal optical phonons in the SiO_2 network. In the earlier study on single Si NCs,[7] this observation was interpreted as exciton-phonon coupling supported by charge carriers trapped at the interface. The fact that identical PL spectra are observed from single SiO_2 NPs[22] queries this interpretation and poses the question whether excitons were involved at all.

(3) Both Si NCs and SiO_2 NPs are characterized by the same rather short lifetime of approximately 4 ns. This is in sharp contrast to the expected lifetime of $\sim$20 μs for the majority of Si NCs if QC PL were operative. Another interesting result of the present work is the fact that phonon coupling does not promote the photoemission as it would be expected for QC PL of Si NCs due to their indirect band gap structure, i.e., there is no phonon-assisted effect.

(4) Remarkably, the majority of single-particle PL spectra measured for both systems are preferably observed in the energy range between 2.0 and 2.5 eV while the PL spectrum of the ensemble of Si NCs, from which the microscopy samples were prepared, peaks at 1.5 eV. According to Wolkin *et al.*,[4] this energy range can only be accessed by oxidized Si NCs if the diameter of the core becomes smaller than 2 nm. A simple explanation can be based on the impact of the preparation method. It could be possible that due to the dispersion in toluene, the Si NCs have suffered additional oxidation so their cores have shrinked below 2 nm in diameter giving rise to electron trapping at oxygen-related defects.[4,7] An alternative explanation could be ascribed to the polymer matrix surrounding the oxide-covered Si NCs and defects created at this new interface.

(5) The latter scenario also offers an alternative explanation of the phonon side bands. If the defects are located at the interface between the oxide layer and the polymer matrix, they could easily couple to molecular vibrations of functional groups in the matrix material. In both polymers used, CH_3 and CH_2 groups are present, which could be responsible for side bands in the energy range between 140 and 180 meV, as observed in the present study.

Summarizing the results just discussed, we conclude that the PL observed for single Si NCs embedded in polymer matrices always originated from defects. Only when we prepared the samples by depositing single Si NCs in a cluster beam apparatus were we able to observe PL, which can be ascribed to the radiative recombination of quantum-confined excitons. This interpretation is based on the following three observations: (1) The single-particle PL spectra have their maxima between 680 and 750 nm. This is the energy range (1.65–1.8 eV) which is actually predicted[41] for the band gaps of Si NCs with diameters between 3.4 and 4.1 nm used in the present study. (2) The band positions measured for single Si NCs comply with the overall ensemble spectrum of a thick Si NC sample produced during the same run. (3) Finally, the Si NC fluorescence occurs on the same time scale, as observed in earlier ensemble lifetime measurements[28,50] and as predicted by theory.[50] Note that quantum confinement-related PL of *single* Si NCs, produced by a bottom-up technique as constituted by gas-phase condensation and protected by a naturally grown oxide layer, could be characterized in both frequency and time domain. From several investigations on single Si NCs to be discussed below, only the study of Valenta *et al.*[45] revealed similar PL spectra, as far as their shape, position, and width are concerned. In contrast to our approach, these authors applied a top-down method (electron beam lithography and reactive ion etching followed by oxidation) to produce irregularly shaped Si quantum dots, so-called nanopillars.

The scarce literature reporting on the PL properties of *single* silicon quantum dots can be divided into three classes. On the one hand, PL spectra featuring phonon structure were observed in the green-yellow spectral range by Martin *et al.*,[7] El-Kork *et al.*,[38] and Kůsová *et al.*[51] On the other hand, single featureless PL bands of Lorentzian type located in the red or near-infrared spectral ranges have been found by Valenta *et al.*[45,52] Finally, single-particle studies revealing both types of spectra were published by Mason *et al.*[53] and English *et al.*[54] Our studies show that the observation of either kind may depend on the preparation technique but can also be observed concurrently from different nanoparticles that have experienced the same history.

There seems to be general agreement[7,38,53,54] that the phonon peaks with a separation of 160 meV being observed in conjunction with the green-yellow PL have to be attributed to the excitation of Si-O-Si stretching modes. Only in the very recent study by Kůsová *et al.*[51] this interpretation is questioned as these authors have removed the SiO_2 shell from their Si NCs. Taking into account that the respective PL is based on defect centers, as shown by the present study, and that Kůsová and coworkers performed the spectroscopy not only on a single particle but also on a single defect on the surface of

this particle, oxygen-related defect centers cannot be excluded with certainty. In this context, it should also be mentioned that Fourier transform infrared spectroscopy performed for the powder from which the sample was prepared is not sensitive enough to detect functional groups coupling to the defect centers, which may be present in very low concentration. Considering the amazing potential of nanoparticles as single-molecule sensors, this low concentration can still be high enough to govern the PL properties of a single nanoparticle.

Comparing the different results, it is interesting to note that the green-yellow PL that is accompanied by phonon coupling is often observed when the samples were chemically treated, for example, by an etching process, by dispersing them in a solvent, by surface functionalization, or by preparing a polymer host matrix for the NPs. This poses the question whether the chemical treatment could be responsible for the defects seen in the single-particle spectroscopy. Many of the chemicals used contain CH_3 and CH_2 functional groups, and therefore, it may be proposed that these functional groups could also be involved in the observed phonon coupling.

It is indicative that, in the present study, exciton-related PL could not be observed when the Si NCs were embedded in a polymer matrix even though the microscopy setup was already optimized for measuring very weak PL signals. This observation could support the negative role of chemical treatment. In contrast, exciton-related PL could be observed when the microscopy samples were prepared by cluster beam deposition, i.e., without coming into contact with any chemical. In this case, however, defect PL and phonon coupling also could be observed. This observation can be explained by assuming strong or even full oxidation of the smaller Si NCs as a result of their exposed position on the fused quartz window since the Si NC coverage was extremely low.

The mutual role of quantum confinement and surface chemistry has recently been elaborated in a review paper by Sa'ar.[55] The author concludes that both phenomena are responsible for the PL of nanostructured silicon. To explain his experimental results, Sa'ar introduces the so-called vibron model, which involves a resonant coupling between electronic sublevels (in the Si core) and surface vibrations. Single-particle spectra with phonon side bands like the ones shown in Fig. 2 or published by Martin *et al.*[7] seem to support the vibron model. The present results, however, suggest that these spectra must be attributed solely to defect luminescence, without need to invoke exciton-phonon coupling.

IV. CONCLUSIONS

Quantum-confined PL could be observed for single, free-standing, oxygen-passivated Si NCs synthesized by gas-phase condensation, without resorting to any chemical treatment or processing. The single-particle PL spectra are observed in the red-to-infrared spectral range and do not reveal coupling to Si-O-Si phonons. Silicon phonon replica could not be resolved in the present room-temperature spectra. Fluorescence decay measurements, carried out for the first time for single silicon nanoparticles, yielded lifetime values in the μs range. The conclusion was further supported by the observation of a degenerate transition dipole moment for excitation, as could be demonstrated by ringlike fluorescence patterns characteristic for excitonic excitation.

Within the same sample, we found coexistence between Si NCs exhibiting QC PL and others showing defect luminescence. Comparing Si NCs and SiO_2 NPs, embedded in polymer (PMMA or PS), the surrounding dielectric medium is found to have significant influence on the optical properties of the Si NCs. The luminescence arises from defect centers located either at the Si/SiO_2 interface or at the SiO_2/polymer interface promoting a strong electron-phonon coupling. The present results favor Si-O-Si vibrations as the explanation for the phonon side bands, but alternative interpretations cannot be excluded. The close resemblance of Si NC and SiO_2 NP spectra, the observation of a linear transition dipole moment for excitation, and the short lifetime of the order of 4 ns are incompatible with the quantum confinement picture and confirm that the PL is governed by defect centers.

Further studies will focus on questions whether excitonic excitation may couple to a defect center within the same particle and at what characteristic size the distinction between a Si NC with oxide shell and a SiO_2 NP becomes obsolete because the larger volume of the oxide shell starts to dominate the PL properties. To address this issue, efforts will be undertaken to perform PL spectroscopy in combination with Raman spectroscopy and/or high-resolution electron transmission microscopy, in order to determine the internal structure of the very same NP that has been optically characterized in the confocal microscope.

ACKNOWLEDGMENTS

This work was carried out within the European cooperation NANOLUM. F. H. and T. S. are grateful for the support by the Max Planck Society and the European Commission (Specific Targeted Project: BONSAI, Contract No. LSHB-CT-2006-037639). A.I.C., A.M.C., and A.J.M. acknowledge financial support by the Forschungsschwerpunktprogramm Baden-Württemberg and from the European Commission through the Human Potential Program (Marie-Curie Research Training Network NANOMATCH, Contract No. MRTN-CT-2006-035884).

*These authors contributed equally to this work.
†Present address: Material Physics, ICT School, Royal Institute of Technology (KTH), Electrum 229, SE-164 40 Kista-Stockholm, Sweden.
‡Present address: III. Institute of Physics, Georg August University Göttingen, D-37077 Göttingen, Germany.
§alfred.meixner@uni-tuebingen.de
‖Corresponding author: friedrich.huisken@uni-jena.de

[1] L. Canham, Appl. Phys. Lett. **57**, 1046 (1990).
[2] V. Lehmann and U. Goesele, Appl. Phys. Lett. **58**, 856 (1991).
[3] B. Delley and E. F. Steigmeier, Phys. Rev. B **47**, 1397 (1993).
[4] M. V. Wolkin, J. Jorne, P. M. Fauchet, G. Allan, and C. Delerue, Phys. Rev. Lett. **82**, 197 (1999).
[5] A. Puzder, A. J. Williamson, J. C. Grossman, and G. Galli, Phys. Rev. Lett. **88**, 097401 (2002).

[6]J. Heitmann, F. Müller, M. Zacharias, and U. Gösele, Adv. Mater. **17**, 795 (2005).
[7]J. Martin, F. Cichos, F. Huisken, and C. von Borczyskowski, Nano Lett. **8**, 656 (2008).
[8]Y. D. Glinka, S. H. Lin, L. P. Hwang, and Y. T. Chen, Appl. Phys. Lett. **77**, 3968 (2000).
[9]U. Gösele, Nat. Nanotech. **3**, 134 (2008).
[10]S. Godefroo, M. Hayne, M. Jivanescu, A. Stesmans, M. Zacharias, O. I. Lebedev, G. van Tendeloo, and V. V. Moshchalkov, Nat. Nanotech. **3**, 174 (2008).
[11]R. Walters, G. Bourianoff, and H. Atwater, Nat. Mater. **4**, 143 (2005).
[12]L. Pavesi, L. Dal Negro, C. Mazzoleni, G. Franzo, and F. Priolo, Nature **408**, 440 (2000).
[13]H. Rong, A. Liu, R. Jones, O. Cohen, D. Hak, R. Nicolaescu, A. Fang, and M. Paniccia, Nature **433**, 292 (2005).
[14]E.-C. Cho, S. Park, X. Hao, D. Song, G. Conibeer, S.-C. Park, and M. A. Green, Nanotechnology **19**, 245201 (2008).
[15]H. Bahruji, M. Bowker, and P. R. Davies, Int. J. Hydrogen Energy **34**, 8504 (2009).
[16]L. Wang, V. Reipa, and J. Blasic, Bioconjugate Chem. **15**, 409 (2004).
[17]F. Erogbogbo, K.-T. Yong, I. Roy, G. Xu, P. N. Prasad, and M. T. Swihart, ACS Nano **2**, 873 (2008).
[18]J.-H. Park, L. Gu, G. von Maltzahn, E. Ruoslahti, S. N. Bhatia, and M. J. Sailor, Nat. Mater. **8**, 331 (2009).
[19]G. Ledoux, O. Guillois, F. Huisken, B. Kohn, D. Porterat, and C. Reynaud, Astron. Astrophys. **377**, 707 (2001).
[20]M. H. Nayfeh, S. R. Habbal, and S. Rao, Astrophys. J. **621**, L121 (2005).
[21]L. Pavesi and R. Turan, eds., *Silicon Nanocrystals: Fundamentals, Synthesis and Applications* (Wiley-VCH-Verlag, Weinheim, 2010).
[22]A. M. Chizhik, A. I. Chizhik, R. Gutbrod, A. J. Meixner, T. Schmidt, J. Sommerfeld, and F. Huisken, Nano Lett. **9**, 3239 (2009).
[23]L. Novotny, M. R. Beversluis, K. S. Youngworth, and T. G. Brown, Phys. Rev. Lett. **86**, 5251 (2001).
[24]R. Dorn, S. Quabis, and G. Leuchs, Phys. Rev. Lett. **91**, 233901 (2003).
[25]M. Ehbrecht and F. Huisken, Phys. Rev. B **59**, 2975 (1999).
[26]G. Ledoux, O. Guillois, D. Porterat, C. Reynaud, F. Huisken, B. Kohn, and V. Paillard, Phys. Rev. B **62**, 15942 (2000).
[27]F. Huisken, H. Hofmeister, B. Kohn, M. A. Laguna, and V. Paillard, Appl. Surf. Sci. **154-155**, 305 (2000).
[28]F. Huisken, G. Ledoux, O. Guillois, and C. Reynaud, Adv. Mater. **14**, 1861 (2002).
[29]A. M. Chizhik, T. Schmidt, A. I. Chizhik, F. Huisken, and A. J. Meixner, Proc. SPIE **7393**, 739305 (2009).
[30]F. Huisken, D. Amans, O. Guillois, G. Ledoux, C. Reynaud, H. Hofmeister, F. Cichos, and J. Martin, New J. Phys. **5**, 10 (2003).
[31]See Supplemental Material at http://pubs.acs.org/doi/suppl/10.1021/nl901509k/suppl_file/nl901509k_si_001.pdf.
[32]L. E. Brus, P. F. Szajowski, W. L. Wilson, T. D. Harris, S. Schuppler, and P. H. Citrin, J. Am. Chem. Soc. **117**, 2915 (1995).
[33]S. A. Empedocles, R. Neuhauser, and M. G. Bawendi, Nature **399**, 126 (1999).
[34]A. I. Chizhik, A. M. Chizhik, D. Khoptyar, S. Bär, and A. J. Meixner, Nano Lett. **11**, 1131 (2011).
[35]H. Hofmeister, F. Huisken, and B. Kohn, Eur. Phys. J. D **9**, 137 (1999).
[36]See Supplemental Material at http://link.aps.org/supplemental/10.1103/PhysRevB.86.125302 for experimental details and additional results on the defect PL of Si NCs.
[37]F. Gourbilleau, X. Portier, C. Ternon, P. Voivenel, R. Madelon, and R. Rizk, Appl. Phys. Lett. **78**, 3058 (2001).
[38]N. El-Kork, F. Huisken, and C. von Borczyskowski, J. Appl. Phys. **110**, 074312 (2011).
[39]G. Ledoux, J. Gong, F. Huisken, O. Guillois, and C. Reynaud, Appl. Phys. Lett. **80**, 4834 (2002).
[40]I. Mihalcescu, J. C. Vial, and R. Romestain, J. Appl. Phys. **80**, 2404 (1996).
[41]C. Delerue, G. Allan, and M. Lannoo, Phys. Rev. B **48**, 11024 (1993).
[42]J. A. Rowlette, R. D. Kekatpure, M. A. Panzer, M. L. Brongersma, and K. E. Goodson, Phys. Rev. B **80**, 045314 (2009).
[43]Z. Lin, H. Li, A. Franceschetti, and M. T. Lusk, ACS Nano **6**, 4029 (2012).
[44]O. Guillois, G. Ledoux, F. Huisken, N. Herlin-Boime, and C. Reynaud, J. Appl. Phys. **95**, 3677 (2004).
[45]J. Valenta, R. Juhasz, and J. Linnros, Appl. Phys. Lett. **80**, 1070 (2002).
[46]I. Sychugov, R. Juhasz, J. Valenta, and J. Linnros, Phys. Rev. Lett. **94**, 087405 (2005).
[47]I. Sychugov, J. Valenta, K. Mitsuishi, M. Fujii, and J. Linnros, Phys. Rev. B **84**, 125326 (2011).
[48]C. Delerue, G. Allan, and M. Lannoo, Phys. Rev. B **64**, 193402 (2001).
[49]D. Kovalev, H. Heckler, G. Polisski, and F. Koch, Phys. Status Solidi B **215**, 871 (1999).
[50]C. Delerue, G. Allan, C. Reynaud, O. Guillois, G. Ledoux, and F. Huisken, Phys. Rev. B **73**, 235318 (2006).
[51]K. Kůsová, O. Cibulka, K. Dohnalová, I. Pelant, J. Valenta, A. Fučiková, K. Žídek, J. Lang, J. Englich, P. Matějka, P. Štěpánek, and S. Bakardjieva, ACS Nano **4**, 4495 (2010).
[52]J. Valenta, A. Fučiková, F. Vácha, F. Adamec, J. Humpolíčková, M. Hof, I. Pelant, K. Kůsová, K. Dohnalová, and J. Linnros, Adv. Funct. Mater. **18**, 2666 (2008).
[53]M. D. Mason, G. M. Credo, K. D. Weston, and S. K. Buratto, Phys. Rev. Lett. **80**, 5405 (1998).
[54]D. S. English, L. E. Pell, Z. H. Yu, P. F. Barbara, and B. A. Korgel, Nano Lett. **2**, 681 (2002).
[55]A. J. Sa'ar, Nanophotonics **3**, 032501 (2009).